Phys Chem Minerals (1999) 26:187–197

ORIGINAL PAPER

U.H. Faul · J.D. Fitz Gerald

Grain misorientations in partially molten olivine aggregates: an electron backscatter diffraction study

Received: 8 December 1997 / Revised, accepted: 6 April 1998

Abstract In polycrystalline aggregates of olivine with mean grain sizes above 35 μm plus a low basaltic melt fraction, both wetted and melt-free grain boundaries are observed after equilibration times at high pressures and temperatures of between 15 and 25 days. In order to assess a possible dependence of the wetting behaviour on the relative orientation of neighbouring grains, a SEM based technique, electron backscatter diffraction (EBSD), is used to determine grain orientations. From the grain orientations relative orientations of neighbouring grains are calculated, which are expressed as misorientation axis/angle pairs. The distribution of misorientation angles and axes of melt-free grain boundaries differ significantly from a purely random distribution, whereas those of wetted grain boundaries are statistically indistinguishable from the random distribution. The relative orientation of two neighbouring grains therefore influences the character of their common grain boundary. However, no clustering towards special (coincident site lattice) misorientation axes is observed, with the inference that the energy differences between special and general misorientations are too small to lead to the development of preferred misorientations during grain growth.

Key words Partial melt · Grain boundary · Olivine · Misorientation · Electron backscatter diffraction

Introduction

The structure and properties of grain boundaries in rocks significantly contribute to their bulk physical properties, ranging from seismic velocities (e.g. Tan et al. 1997), electrical conductivity (e.g. Roberts and Tyburczy 1991), diffusivities (e.g. Farver et al. 1994) to the distribution of melt (e.g. Faul 1997; Cmíral et al. 1998). Despite their significance, only the structure of low-angle grain boundaries (subgrain boundaries) in polycrystalline olivine aggregates has been investigated in detail (Ricoult and Kohlstedt 1983a, b). They found that the mismatch of neighbouring lattices across subgrain boundaries with misorientations $<2°$ is accommodated by regularly spaced dislocations. Most grain boundaries in natural rocks have misorientations $>15°$, for which the associated lattice mismatch cannot be as easily accommodated by simple dislocation structures. Only a few high resolution images (lattice fringe images in a transmission electron microscope, TEM) of high angle grain boundaries have been published (e.g. Cooper and Kohlstedt 1982; Vaughan et al. 1982), mostly of boundaries involving (020) planes which have the largest spacing and are the easiest to observe.

An indication of the diversity of the grain boundary structure of polycrystalline olivine is given by the melt distribution in partially molten aggregates. For a partially molten system under hydrostatic conditions the melt distribution is the result of minimisation of interfacial energies locally through the wetting behaviour and overall by a reduction in the grain surface area through grain growth. In a transmission electron microscope study of the wetting behaviour at high magnification, we found that subgrain boundaries have large wetting angles ($>90°$) and are melt-free, whereas wetting angles for general (high angle) grain boundaries are variable, ranging from 0° to 40° (Cmíral et al. 1998). In this range most angles are $<10°$, only angles formed by two faceted grain boundaries are $>10°$. At melt contents of a few percent most of the volume of melt resides in layers on two-grain boundaries and larger pockets or interserts, but not all grain boundaries are wetted (Faul et al. 1994; Faul 1997). At low melt contents ($<1\%$) most grain boundaries are melt free at a resolution to about 10 nm. With increasing melt fraction more and more grain boundaries are wetted by melt; at melt contents of 2–3% more than half of the two-grain boundaries are separated by a melt layer. These observations are made from samples that have been equilibrated under hydrostatic conditions at high temperatures and pressures for up to 25 days, and have under-

Ulrich H. Faul (✉) · John D. Fitz Gerald
Research School of Earth Sciences,
The Australian National University, Canberra ACT 0200, Australia
e-mail: uli.faul@anu.edu.au
Fax: +61-2-6249-3414

gone significant grain growth. The presence of both wetted and melt free grain boundaries therefore represents adjustments of the system to lower the surface energy.

An interface or grain boundary between two crystals has five macroscopic degrees of freedom: three due to the relative orientation of the neighbouring crystal lattices and two due to the orientation of the grain boundary plane (e.g. Sutton and Balluffi 1987). This provides a geometric description of the grain boundary where physical interactions between atoms at the interface (or microscopic degrees of freedom) are not taken into account. In the macroscopic description of the grain boundary, the interface seeks to minimise its free energy in this five-parameter space. This study examines three of these parameters, looking for correlations of the relative orientation of neighbouring olivine grains with the occurrence of wetted versus melt-free grain boundaries. To cover the full range of possible orientation relationships of general grain boundaries a large number needs to be examined. To do this at random by TEM would be prohibitively time consuming. A scanning electron microscope (SEM) based technique to determine grain orientations, electron backscatter diffraction (EBSD), allows much more data to be collected in a reasonable amount of time. Further, in the SEM the complete sample can be examined, avoiding the limitations of the ion beam milling process necessary to produce thin sample areas for the TEM. However, without serial sectioning the full grain boundary orientation cannot be determined with the SEM. For the purpose of this study we therefore only investigate grain misorientations and not grain boundary plane orientations. Finally, due to the limited resolution of SEMs, melt films less than $\sim$5 nm wide (e.g. Drury and Fitz Gerald 1996) are not considered here.

Electron backscatter diffraction

By observing electron diffraction patterns in the SEM it is possible to record a large scattering angle (e.g. Randle 1992, Figure 1.1), which is especially important for identification of the more complex patterns from materials with symmetries lower than cubic. The patterns are generated by inelastic interaction of the incident electron beam with the sample, which scatters the electrons in a pear-shaped volume. Some of these electrons have the correct angular relationship with the planes of the surrounding crystalline material for coherent (elastic) scattering (Bragg diffraction). Because the initial inelastic scattering generates electrons with a continuous range of directions, a number of planes fulfil the Bragg condition; each plane generates a band of diffracted electron intensity. Together these bands form a pattern which reflects the relationships of the planes in the crystal structure. These patterns can be used to determine the orientation of the crystal relative to the incident beam. To allow most electrons to leave the sample, it is inclined at 70° from the usual horizontal position. An example of an EBSD pattern from olivine is shown in Fig. 1. For a general introduction to EBSD see for example Randle (1992).

Part of the pattern is captured by a low light charge coupleddevice camera from a phosphor screen, enhanced by on-chip frame integration and background subtraction with an Argus 20 image processor, and recorded digitally via a frame grabber card. Depending on pattern quality and symmetry of the material, an automated band detection and indexing procedure can be employed. The EBSD system used for this study at the Electron Microscopy Unit at the Australian National Universiy consists of hardware supplied by Nordif mounted on a JEOL 6400 SEM with conventional Tungsten filament, and the software package Channel+ from HKL software.

The best patterns were recorded at 20 kV acceleration voltage and nominal beam currents of 10 nA. A carbon coat (approximately 10 nm thick) was necessary to avoid charging of the sample. Some contamination by the electron beam is observed in the secondary electron (SE) image; pattern and SE image quality deteriorate slowly in the scanned area. Pattern quality varied from grain to grain, but in most cases automated detection of five to six bands is possible. Detection of fewer than five bands can lead to ambiguities in the following simulation due to the relatively large number of bands present. Patterns

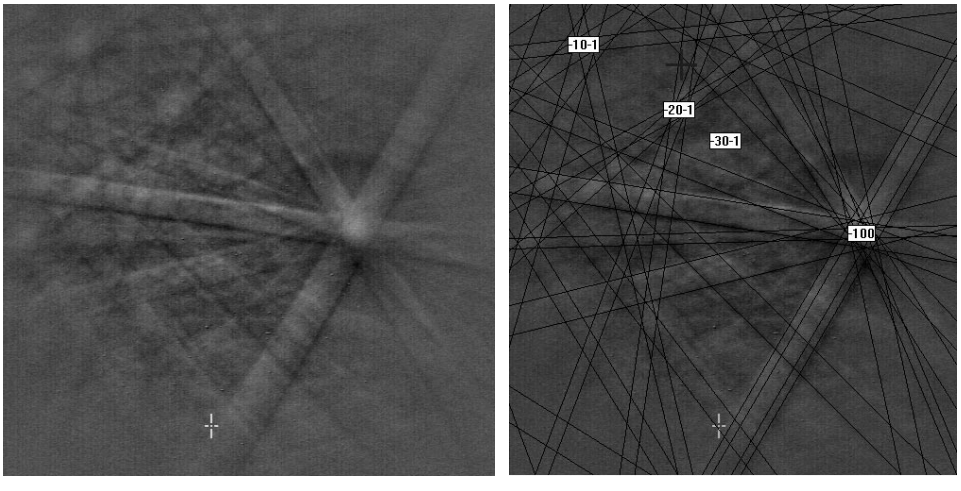

Fig. 1 Example of a raw and indexed EBSD pattern from olivine. Major zone axes are indicated

are simulated from a set of 58 reflectors for the olivine crystal structure (corresponding to a cut-off intensity relative to the brightest band of ~10%, below which the bands are generally no longer visible in the recorded pattern) and compared to the detected bands for indexing. Fully automated pattern acquisition and indexing does not seem possible at this point due to variable pattern quality, as well as due to the difficulty of correctly indexing some patterns, for example near the [011] and [001] zone axes.

Grain orientations are stored as Euler angles as a convenient way to relate the orientation of individual grains to a reference coordinate system (e.g. the sample coordinate system). Euler angles describe a specific sequence of rotations with rotation angles (φ_1, ϕ, φ_2) to transform (or rotate) one coordinate system to another (see for example Goldstein 1980). These rotations can also be described in matrix form and multiplied together to an orientation matrix **O** (Goldstein 1980; Randle 1992, 1993, and references therein):

$$\mathbf{O}^{-1} = \begin{pmatrix} \cos\varphi_2 & \sin\varphi_2 & 0 \\ -\sin\varphi_2 & \cos\varphi_2 & 0 \\ 0 & 0 & 1 \end{pmatrix} \begin{pmatrix} 1 & 0 & 0 \\ 0 & \cos\phi & \sin\phi \\ 0 & -\sin\phi & \cos\phi \end{pmatrix} \cdot \begin{pmatrix} \cos\varphi_1 & \sin\varphi_1 & 0 \\ -\sin\varphi_1 & \cos\varphi_1 & 0 \\ 0 & 0 & 1 \end{pmatrix} \quad (1)$$

The columns of **O** are the Cartesian coordinates of the crystal axis in the sample coordinate system.

The most common way to express the orientation relation of two neighbouring grains is by a misorientation axis/angle pair. The axis of misorientation is a direction which has the same Miller indices in both crystal coordinate systems (e.g. Randle 1992). Taking the orientation of one grain as a fixed reference system, the misorientation angle describes how far the second grain has to be rotated about the common axis to bring its coordinate system into coincidence with the first grain. Equivalently, the relative orientation of the two grains could be expressed by Euler angles, but the advantages of the misorientation axis/angle pair description are that low angle and special grain boundaries can be recognised more easily.

The misorientation axis/angle pair [uvw]/(θ) is calculated from the misorientation matrix **M** from the orientation matrices of two grains (e.g. Randle 1992, 1993)

$$\mathbf{M} = \mathbf{O}_1^{-1}\mathbf{O}_2 \quad (2)$$

as:

$$u = M_{23} - M_{32}, \quad v = M_{31} - M_{13}, \quad w = M_{12} - M_{21}, \quad (3)$$

$$\cos\theta = (M_{11} + M_{22} + M_{33} - 1)/2 \quad (4)$$

For the orthorhombic system there are four equivalent ways to index each grain, resulting in 16 axis/angle pairs. These 16 pairs are comprised of four symmetrically equivalent sets with four different angles. The four different axis/angle pairs are obtained by multiplying **M** with the following matrices:

$$\begin{pmatrix} 1 & 0 & 0 \\ 0 & 1 & 0 \\ 0 & 0 & 1 \end{pmatrix}, \begin{pmatrix} 1 & 0 & 0 \\ 0 & -1 & 0 \\ 0 & 0 & -1 \end{pmatrix}, \begin{pmatrix} -1 & 0 & 0 \\ 0 & 1 & 0 \\ 0 & 0 & -1 \end{pmatrix}, \begin{pmatrix} -1 & 0 & 0 \\ 0 & -1 & 0 \\ 0 & 0 & 1 \end{pmatrix}.$$

As the four different axis/angle pairs are physically indistinguishable from the orientation measurement, commonly the one with the smallest angle is chosen (sometimes called disorientation, Grimmer 1979, 1980). In the following always the smallest angle and corresponding axis is used but referred to simply as misorientation.

A measure of the uncertainty in grain orientations relative to each other is given by the software as mean angular deviation (MAD) between detected bands and simulated patterns. This error is mainly due to uncertainties in the relative positions and orientations of sample surface and phosphor screen. Generally MAD values are kept below 1° by calibration and refinement of the accuracy of the orientations and positions. In addition there is a systematic error of each grain orientation with respect to the sample coordinate system. This systematic error results from the uncertainty of the sample orientation relative to the microscope axes, which varies slightly every time the sample is inserted into the SEM. To avoid this systematic error, misorientations were calculated only between grain orientations determined in the same SEM session.

Experimental details and data acquisition

The starting material for the experiments consisted of hand-picked and finely ground olivine from Mt. Porndon, Victoria; sieved to below 25 µm. The mean grain size of the starting powder is considerably smaller, as the grinding produces numerous micron and submicron-sized fragments. A small fraction of oxide derived sintered powder with basaltic composition was added to provide the melt phase at run conditions. All samples were run in a 1/2″ piston cylinder apparatus at 1 GPa pressure with NaCl-pyrex outer sleeves, graphite heater and internal spacers of crushable MgO (60% dense). The samples were encapsulated in graphite with outer capsules of Pt. Run temperatures varied between 1360° and 1410°C, and run durations ranged from 379 to 612 h. Details of sample preparation, furnace assembly and composition of sample material are given by Faul (1997) and Cmíral et al. (1998). The experimental conditions are summarised in Table 1.

The sample capsules were sectioned vertically after the run and polished first with diamond to flatten the surface, then with 0.05 µm alumina powder and as a last step with colloidal silica. A completely undamaged surface (top few nm) is necessary for EBSD patterns to develop. The quality of the polish can be assessed to some degree from normal SEM backscattered electron (BSE) imaging. Well polished olivine shows orientation contrast at 15 to 20 kV acceleration voltage and beam currents of 3 to 4 nA (Fig. 2). The orientation contrast derives from the same sample-beam interaction process as the generation of the EBSD patterns but can not be used to determine the absolute orientation of the grains. While the orientation contrast enables identification of (melt-free) grain boundaries, the relatively high beam currents decrease the image resolution.

Table 1 Experimental conditions, grain sizes and melt fractions. The pressure of all experiments was 1 GPa

	T, °C	Duration, h	Starting grain size, μm[a]	Grain size after run, μm[b]	Approx. melt content, %
OB29	1410	481	<25	38	3
OB31	1380	379	<25	n.d.	1
OB32	1360	612	<25	43	2

[a] From sieving
[b] Mean value of average of smallest and largest dimension of >200 grains multiplied by 1.5

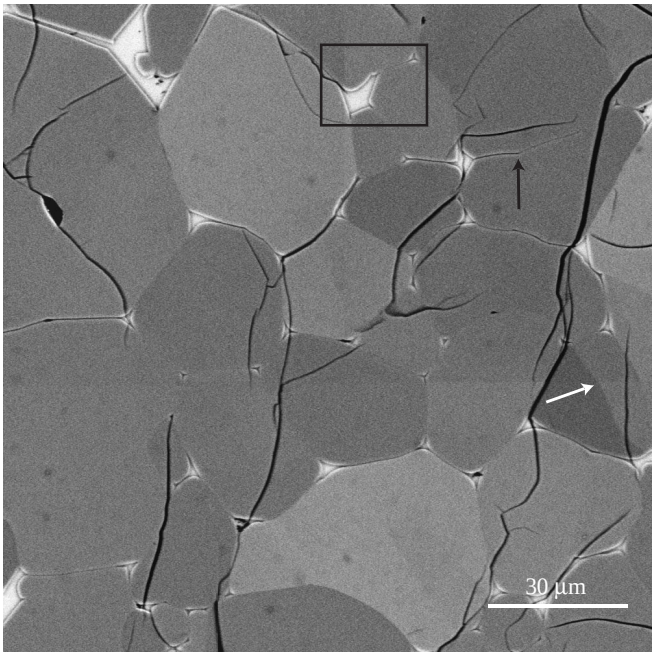

Fig. 2 BSE image of run OB32 showing orientation contrast of olivine. The intergranular melt (now glass) is *light grey*, quench cracks are *black*. The *white arrow* points to a subgrain boundary, the *black arrow* to a melt layer which changes in width and direction due to a subgrain boundary (not visible in this image) intersecting the grain boundary. The *black rectangle* indicates the area shown in Fig. 3

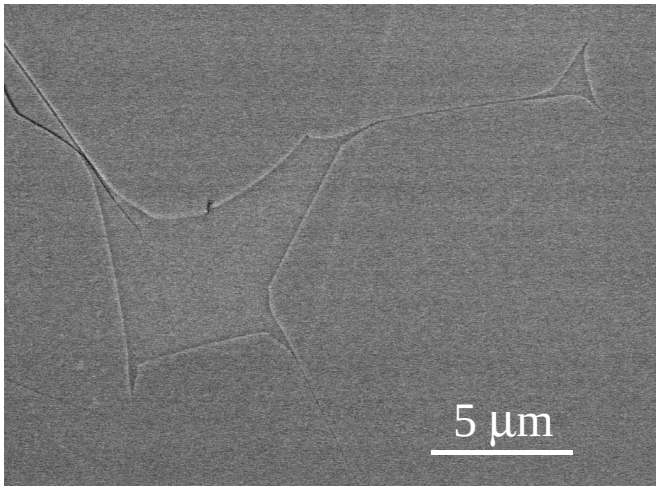

Fig. 3 FESEM-SE image with detail from Fig. 2. This image shows continuous layers of uniform thickness as well as grain boundaries where no melt can be resolved. The layer extending to the upper left can be identified in the BSE image in Fig. 2; it has an approximate thickness of 100 nm. The grain boundary leading to the bottom centre appears melt-free in Fig. 2; the layer has an estimated thickness of 30 nm. FESEM imaging indicates that the majority of layers falls between a few tens and a few hundred nm in thickness

Selected areas of the samples were imaged to map grain and melt distribution. These maps were then used to record the index of each grain in the list of Euler angles to identify neighbouring grains. Because melt layers of 100 nm or less in width cannot be resolved with a conventional SEM, all grain boundaries were examined with a field emission SEM (FESEM, Hitachi 4500). With FESEM imaging layers to about 10 nm in thickness can be detected; Fig. 3 shows examples of layers of different thickness. Imaging conditions were 8 kV acceleration voltage, 13 pA beam current and 7 mm WD.

EBSD results

Sample characteristics

Grain orientation data were collected from three samples. All samples had the same starting material and similar experimental run conditions, with slightly different run durations and melt fractions (Table 1). The mean grain sizes of all three samples were similar in the range around 40 μm, indicating that significant grain growth had taken place. As in earlier experiments (Faul 1997) very little melt resided in tubules along three-grain edges; most of the melt was found in layers on two-grain boundaries and larger pockets or interserts. Layers were present in all samples, but the sample with the lowest melt content (OB31, ~1%) had fewer than OB32 or OB29 with melt contents between 2% and 3%. Correspondingly the number of wetted grain boundaries was significantly higher in the latter two samples.

Layers are defined as being more than about 5 nm wide to distinguish them from films, for which the width is controlled by the balance of short range attractive and repulsive forces (Clarke 1987). The range of these forces for the present system is not exactly known, but most film thicknesses reported from other ceramic systems fall in the range from 1 to 5 nm. For olivine our observations indicate that only a few exceed 2 nm in width (Drury and Fitz Gerald 1996). Both FESEM and TEM observations indicate that layers generally have a constant width (i.e. the grain surfaces are parallel to each other) and are frequently curved (Fig. 3). A change in the width of a layer seems always associated with a subgrain boundary intersecting the layer (black arrow in Fig. 2).

The majority of the layers are between 20 and a few 100 nm wide. The upper limit on the thickness of layers

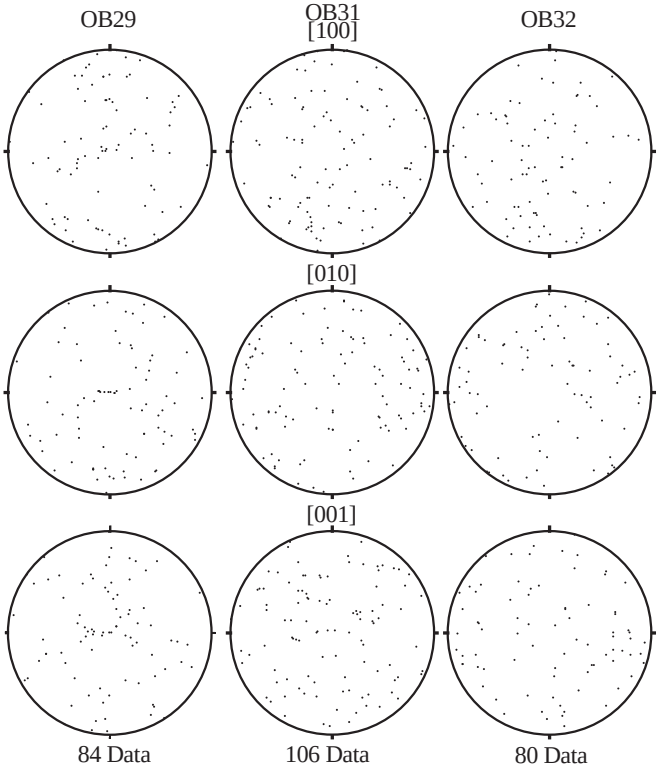

Fig. 4 Pole figures (lower hemisphere equal area) of grain orientations determined by EBSD show no preferred alignment of grains. For OB29 and OB32 only a subset of orientations, all obtained in the same SEM session, is shown

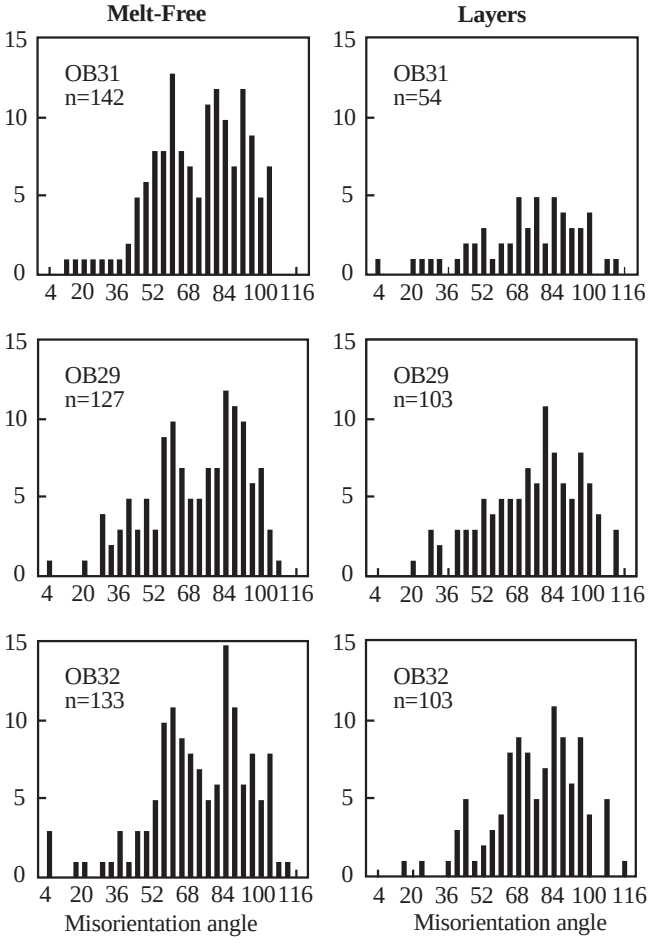

Fig. 5 Histograms of misorientation angles from three experiments, divided into melt-free grain boundaries (*left*) and two-grain boundaries separated by a layer of melt (*right*)

is about 1 μm; for wider pockets (interserts) in most cases one or both of the crystal-melt interfaces are faceted and the grain surfaces no longer parallel. For these cases no relation between neighbouring grains is expected and misorientation angles were not calculated. However, this distinction between melt pocket and layer is not always unambiguous, for example for layers where one of the grain boundaries involved appears faceted but the layer appears to have a constant thickness. Because crystal-melt interfaces at larger pockets are not considered in the misorientation data, the relative number of misorientations for wetted versus melt-free grain boundaries is not an absolute measure for the proportion of wetted versus melt-free grain boundary area.

Pole figures of the [100], [010], and [001] axes of individual grains from all three samples show no preferred orientation (Fig. 4), as is expected for hydrostatic conditions. To assess the randomness of a relatively small number of single orientation data more quantitatively, a texture index (J) can be calculated by using the 1/n law method (where n gives the number of individual orientations), (D. Mainprice, personal communication). J at 1/n=0 corresponds to an extrapolation to an infinite number of measurements; for a random distribution J=1. The values for the texture index confirm that the grains in OB29 (J=1.58±0.08) and OB31 (J=1.1±0.1) are randomly oriented, while OB32 has a weak texture (J=3.1±0.3).

Misorientation angles

Histograms of misorientation angles from the three samples are shown in Fig. 5. The grain boundaries are grouped into melt-free (left-hand column) and wetted grain boundaries (right). Melt-free in this context indicates that no melt layer is present at the two-grain boundary that can be resolved by FESEM; wetted indicates that a layer is present. The distributions of the misorientation angles of the melt-free grain boundaries of all three runs are similar, with two more prominent maxima at 60° and 84°. Obvious subgrains (e.g. white arrow in Fig. 2) with misorientation angles generally less than or equal to 2° were excluded from the data; angles in the bin centred on 4° represent neighbouring grains, which touch each other but clearly show some necking at the common grain boundary. The right-hand column of Fig. 5 shows the distribution for two-grain boundaries separated by melt layers. Except for OB31 where the data for wetted grain boundaries is limited, the distributions again show a maximum at or near 84°; but the maximum at 60° is absent.

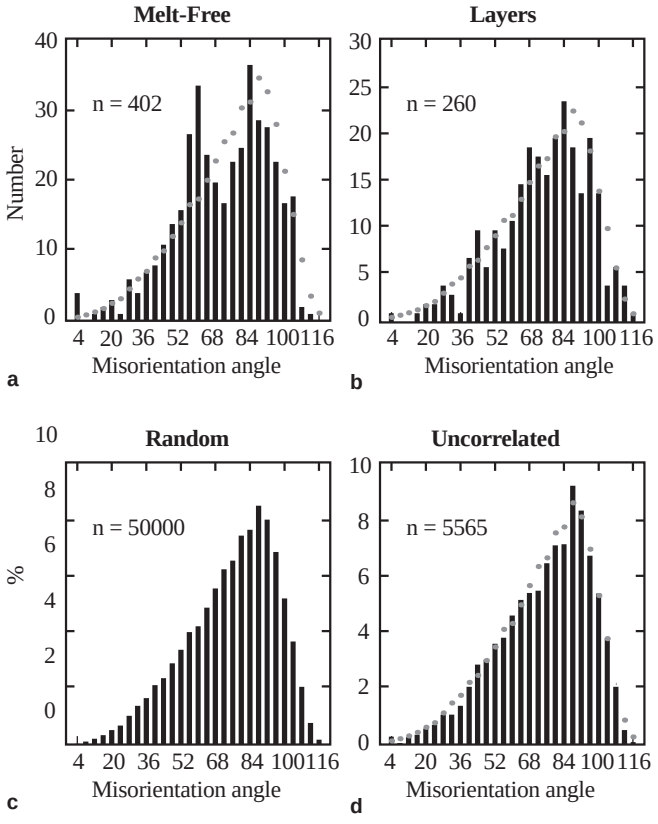

Fig. 6a–d Combined histograms of misorientation angles from three experiments (**a** melt-free, **b** layers), simulated distribution for random misorientations (**c**) and uncorrelated distribution (**d**). The distribution in **d** is calculated from 106 grain orientations from OB31; the uncorrelated distributions from the other two runs are very similar. The random distribution in **c** is also indicated in **a**, **b** and **d** by *grey dots*, in each case normalised to the same number of data as in the histogram. The prominent peak at 60° for the melt-free grain boundaries is absent from the random distributions, whereas the distribution for grain boundaries separated by layers is close to the random distribution of misorientation angles

In order to assess the significance of the distributions obtained from the experimental samples they need to be compared to the distributions expected for random orientations of pairs of grains. In Fig. 6 the combined data from all three experiments, separated into melt-free (Figure 6a) and wetted grain boundaries (Fig. 6b) are compared with two types of random distributions. The distribution in Fig. 6c is derived by calculating the misorientation angles of 50,000 pairs of randomly oriented grains. The simulated distribution increases towards a maximum in the bin centred on 88°, then rapidly decreases towards the maximum possible angle of 120°. Misorientations with angles >120° always have a symmetrically related misorientation axis with a smaller angle (Grimmer 1979, 1980). This simulated distribution matches that for random misorientation angles for the orthorhombic crystal systems given by Grimmer (1979) and Morawiec (1995), with a maximum at 90°, mean=75.1°, standard deviation=20.8° and skewness=–0.62.

The distribution shown in Fig. 6d is obtained from calculating the misorientation of every grain in the data set of one sample relative to every other grain in the set, regardless of whether the grains are physically adjacent to each other or not (uncorrelated distribution, Mainprice et al. 1993; Fliervoet et al. 1998). The distributions thus obtained for the three experiments are nearly indistinguishable from the simulated random distribution in Fig. 6c; consistent with the random orientation of the grains in the samples (Fig. 4). Differences between the distributions for neighbouring grains (Fig. 6a, b) and the random distribution (Fig. 6c) are therefore not due to a preferred orientation. Comparison of these different distributions indicates that the first maximum of the melt-free grain boundaries at 60° is different from the random distribution. The distribution for wetted grain boundaries is, with some fluctuations, similar to the random distribution.

To establish whether the experimentally observed distributions are statistically distinguishable from the distribution for randomly oriented grains, a χ^2 test was used (e.g. Cheeney 1983). To ensure sufficient numbers of data in all bins for the χ^2 test, neighbouring bins in Fig. 6a, b with less than 10 angles were combined so that all bins contain at least 10 data. The number of degrees of freedom is then given by the resulting number of bins minus one for the normalisation of the random distribution to the same total number of observations. The calculated χ^2 values are 38.1 and 10.7 for melt-free and wetted grain boundaries respectively. It follows that for 17 degrees of freedom the distribution of melt-free grain boundaries is different from the random distribution with 99% confidence (critical value of 33.5), whereas the distribution for grain boundaries with layers is indistinguishable from random with 80% confidence (critical value of 12.0).

Misorientation axes

The misorientation axes for melt-free and wetted two-grain boundaries are shown in Fig. 7a, b as lower hemisphere, equal area stereographic projections. Because of symmetric equivalence all misorientation axes are mapped into one quadrant. No obvious clustering is observed. To quantify whether the axes distribution is indeed random the unit triangle is divided into 10 fields as shown in Fig. 7c. The value in each field indicates the expected percentage of axes for a random distribution, calculated from the simulated distribution of 50,000 pairs of grains. A χ^2 test confirms that both melt-free and wetted axes distributions are indistinguishable from the random distribution.

Figures 8 and 9 show the misorientation axes sorted by misorientation angle in 10° bins. Since only relatively few angles are in the 5° to 55° range these are grouped together. Also the angle range >105° has not been considered because it contains too few data. The contouring (counting on a sphere) emphasises differences and similarities of the distributions, but maxima near the edges of the unit triangle are somewhat artificial. At misorientation angles >90° all axis orientations are no longer possible for disorientations (minimum angle misorientations) due to sym-

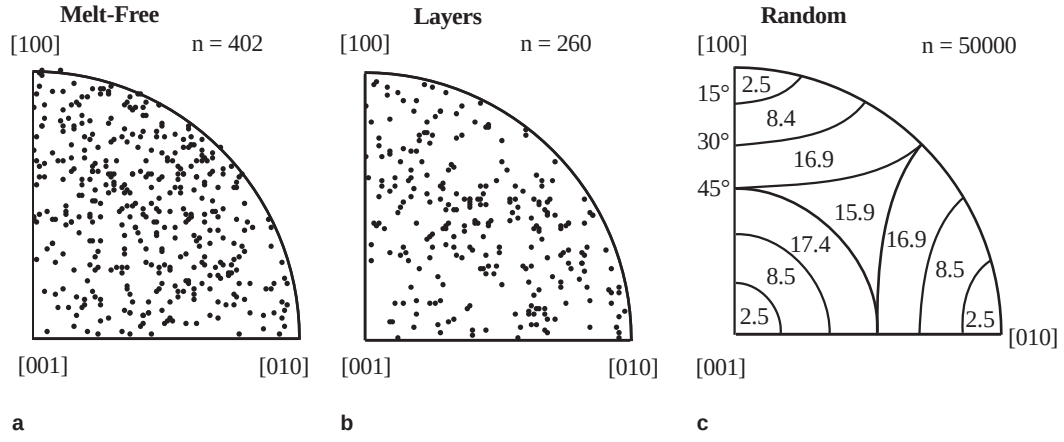

Fig. 7a–c Lower hemisphere, equal area stereographic projection of misorientation axes. All axes are mapped into a unit triangle due to symmetry equivalence. **a** All melt-free grain boundaries. **b** All grain boundaries with layers. **c** Distribution (in percent) from modelling of randomly oriented grains divided into 10 fields. χ^2 tests confirm that both experimental distributions are random

metric equivalence. As an example consider a counterclockwise rotation around [100] by 115°. Because positive and negative crystallographic axes are indistinguishable, a clockwise rotation around [100] by 65° will yield a symmetrically equivalent orientation with a smaller rotation angle. The conditions for possible disorientation axis/angle pairs are given by Grimmer (1980) as:

$$\cos\theta/2 \geq \begin{cases} \cos\xi \sin\theta/2 \geq 0 \\ \cos\eta \sin\theta/2 \geq 0 \\ \cos\zeta \sin\theta/2 \geq 0. \end{cases} \quad (5)$$

ξ, η and ζ are the angles of the misorientation axes with the [100], [010] and [001] axes, respectively. The restricted range of possible axes orientations is indicated in the 95°-105° angle range by concentric contours around the principal crystal axes for 95° and 105°. The clustering of misorientation axes in this angle range is partly due to this effect. Otherwise the misorientation axes are only weakly concentrated, which makes it difficult to ascertain whether the axis distributions are random or not.

To test the misorientation axes distributions again the χ^2 test is used. Due to the limited number of data in each angle range only four fields are compared, from 0° to 45° away from each principal crystal axis, and the centre (see Fig. 7c). Table 2 shows the percentages of axes in each field within each angle range for melt-free grain boundaries. The restricted distribution of axes at angles >90° has been taken into account by comparison with the simulated distribution in the same angle range. This restricted axes distribution gives rise to decreasing percentages in the fields next to the principal crystal axes and an increase in the centre. For three degrees of freedom (the four fields minus one for normalisation) the χ^2 values have to exceed 9.8 for the observed distribution to be different from the random distribution at the 98% confidence level. For melt-free grain boundaries this value is

Table 2 Distribution of misorientation axes sorted by angle for melt-free grain boundaries. All values (except for χ^2) are given in %

Field[a]	[100]	[010]	[001]	Center	χ^2
Random[b] 0–90°	29.0	29.3	29.7	12.0	
5–55°	34.1	28.2	23.5	14.1	2.6
55–65°	44.9	24.6	18.8	11.6	13.5
65–75°	31.3	31.3	14.6	22.9	17.9
75–85°	29.6	25.4	33.8	11.3	1.2
Random 85–95°	28.6	28.9	28.4	13.0	
85–95°	34.3	24.3	28.6	12.9	1.9
Random 95–105°	25.7	25.4	25.9	23.1	
95–105°	36.7	24.5	14.3	24.5	10.1

[a] Field up to 45° away from the indicated axis (see Fig. 7c)
[b] % in each field from modelling of pairs of randomly oriented crystals

exceeded in the angle ranges 55°–65° (coinciding with the first peak of the angle distribution), 65°–75°, as well as 95°–105°; indicating that the strong maximum observed in this last angle range in Fig. 8 is not only due to the restricted axis distribution. The axis distribution in the other angle ranges is close to random. For wetted grain boundaries with a smaller number of total misorientations, some angle ranges had to be combined to yield sufficient data for the χ^2 test (Table 3). Only the axes in the angle range from 85–105° are non-randomly distributed at the 98% confidence level, the distribution of axes in the other angle ranges is close to the random distribution. Thus the melt-free grain boundaries again show a greater tendency towards a non-random distribution as compared to the wetted grain boundaries, although possible concentrations of axes of the wetted grain boundaries might not have been observed due to the small number of data.

Coincident site lattice

Two identical, interpenetrating crystal lattices, where one lattice is rotated with respect to the other one, can gener-

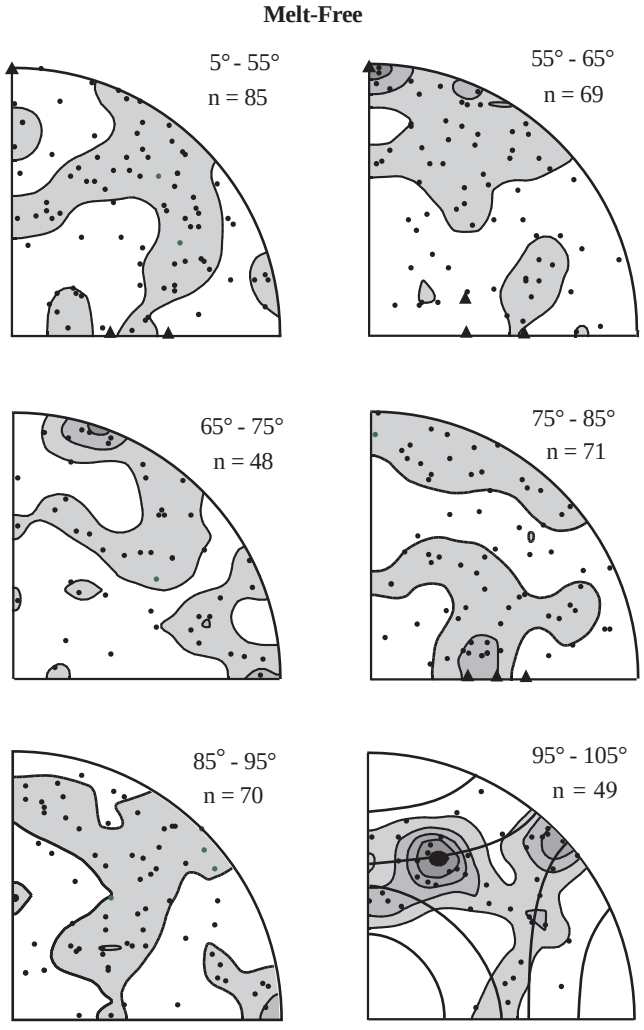

Fig. 8 Stereographic projections of misorientation axes of grains pairs with melt-free grain boundaries divided into six misorientation angle ranges. Individual data points as well as contours are shown. *Triangles* mark CSL misorientation axes in the appropriate angle ranges; for a complete list see Table 4. χ^2 tests show that the angle ranges 55°–65°, 65°–75° and 95°–105° have non-random axis distributions (Table 2). The concentric contours around the [100], [010] and [001] axes in the angle range from 95°-105° indicate "forbidden" areas, the contour closer to the axes refers to 95°, the contours closer to the centre refers to 105°

ate a super-lattice of coincident sites. The periodicity of coincident sites is given by Σ, the reciprocal lattice density. Equivalently 1/Σ gives the fraction of lattice points which coincide. The coincidence site lattice (CSL) concept is a commonly used model to link grain boundary geometry with special properties of certain grain boundaries, particularly for cubic metals (e.g. Randle 1993), but its physical significance for crystals with lower symmetry is less well established (e.g. Babcock and Vargas 1995).

For olivine, (100) planes of oxygen in the orthorhombic crystal structure form an approximately hexagonal close packed (hcp) sub-lattice (Poirier 1975) with an axial ratio $(c/a)^2$ near 5/2, for which coincidence site lattices

Table 3 Distribution of misorientation axes sorted by angle for grain boundaries with layers

Field	[100]	[010]	[001]	Center	χ^2
Random 0–90°	29.0	29.3	29.7	12.0	
5–55°	26.9	28.8	30.8	13.5	0.4
55–75°	27.5	34.8	21.7	15.9	4.5
Random 85–105°	27.4	27.5	28.1	17.0	
85–105°	18.4	40.8	22.4	18.4	10.7

Table 4 Misorientation axis/angle pairs for the oxygen hcp lattice in olivine

Axis	Angles, ° (Σ)							
[100]	60.0 (3)	38.2 (7)	27.8 (13)	46.8 (19)	21.8 (21)	17.9 (31)	50.8 (37)	32.2 (39)
[0 1/3$\sqrt{3}$ 1]	84.8 (11)	57.4 (13)	40.1 (17)	56.9 (22)	34.3 (23)			
[045]	79.8 (17)							
[098]	64.6 (7)	35.1 (11)	76.7 (13)					
[1 5/3$\sqrt{3}$ 5]	65.1 (19)							

have been calculated (see Bollmann 1982, Table M13,3). In non-cubic lattices CSL misorientations can only form for rational axial ratios (e.g. Babcock and Vargas 1995). The axis/angle pairs with axes recalculated from the oxygen hcp structure for the olivine unit cell are given in Table 4 in order of increasing Σ. For rotations around [100], equivalent to [0001] hcp and [111] cubic only CSLs up to Σ=39 are given. The CSL axes are also shown in the appropriate angle ranges on the stereographs in Figs. 8 and 9 as black triangles. Of interest is the peak in the misorientation angle distribution at 60° together with the maximum in the corresponding axis distribution in the angle range from 55° to 65° near [100] (i.e. perpendicular to the basal plane of the hcp lattice). The misorientation axis/angle pair [100]/60° corresponds to a Σ=3 CSL for the oxygen sub-lattice. The corresponding field in Table 2 (angle range 55°–65°, [100]) also shows a concentration of axes significantly above random, but out of the total number of data few are actually close to [100]. The contouring shows a slightly increased concentration of axes near the CSLs in the 75°–85° range but the other CSLs do not have a significant number of axes near them. The peak in the axes distribution in the angle range from 95°–105° is above the maximum possible misorientation angle for the hcp system. Coincident site lattices for the olivine structure itself have not been calculated. Due to the (relatively) low symmetry of olivine, only near coincidences are possible, with additional deformation of the lattice (such as dislocations) necessary to obtain coincidence (Priester 1989).

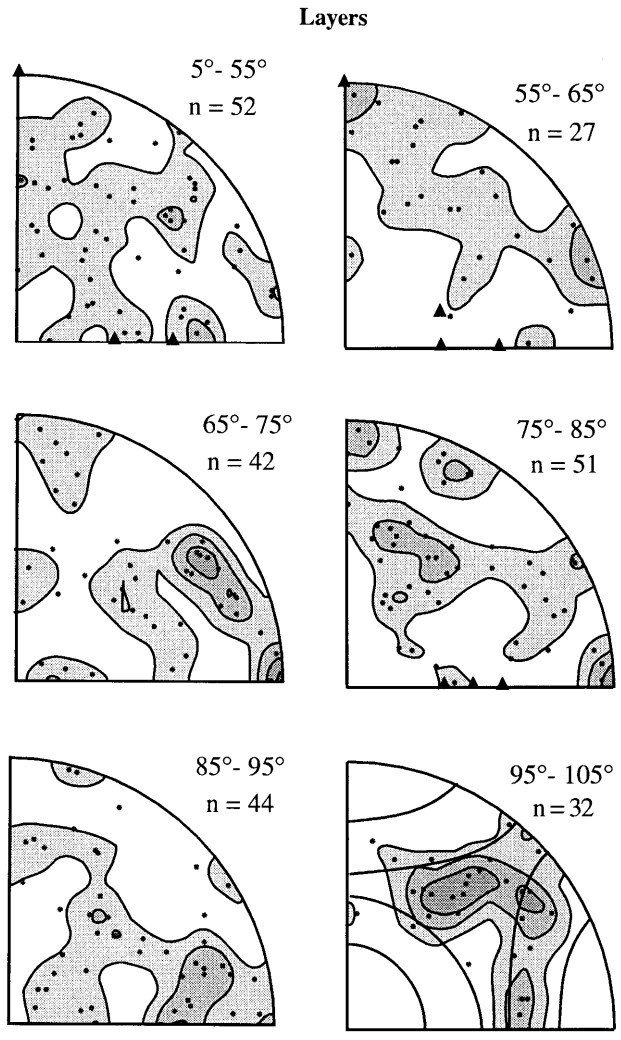

Fig. 9 Stereographic projections of misorientation axes where grains are separated by a layer. Symbols and contours as in Fig. 8. χ^2 tests show that only the axes distribution in the angle ranges from 85°–105° is not random (Table 3)

Discussion

The principal aim of this study was to examine whether there is any correlation between the relative orientation (misorientation) of two neighbouring grains and the observed wetting behaviour of their common boundary, or more precisely, the presence or absence of melt layers on two-grain boundaries. In addressing this question several complicating factors have to be taken into account. Firstly, as pointed out in the introduction, the number of wetted grain boundaries depends on the melt fraction, suggesting that the difference in surface energy between wetted and melt-free grain boundaries is small, at least for some boundaries. Secondly, the majority of grain boundaries, both melt-free and wetted, are curved. This could be due to microfacets at the nanometer scale, but such structures have so far not been reported for olivine, in contrast for example to Al_2O_3 (Shaw and Duncombe 1991; Kim et al. 1994) and cuprate superconductors (Laval and Swiatnicki 1994). Thirdly, the layers have a wide range in thickness, with upper and lower limits which are not always clearly defined, although the number of boundaries with either very thick or very thin layers is probably small.

Melt layers as described here are not unique to the system olivine plus basaltic melt; the combination of layers and melt-free grain boundaries (again not considering films) is also found in other ceramic systems at similar melt fractions. Examples are UO_2–Al_2O_3 (Beere 1975, Fig. 2), quartz plus a silicate melt (Laporte 1994, Fig. 6) and Al_2O_3 plus silicate melt (Shaw and Duncombe 1991, Fig. 6). An intergranular phase up to a few tens of nm thick was also observed on random (general) grain boundaries in $YBa_2Cu_3O_{7-x}$ (Laval and Swiatnicki 1994), for which they infer that the grain boundary energy is minimised by the presence of an intergranular phase. In the penetration experiments of Shaw and Duncombe (1991) cubes of initially melt-free polycrystalline Al_2O_3 were immersed in a silicate melt. After 24 h only grain boundaries with misorientations corresponding to twins remained layer-free. This behaviour is similar to the increasing number of layers with increasing melt fraction for olivine, indicating that the presence of melt lowers the system surface energy as compared to the melt-free aggregate. A physical model for layers, comparable to that presented by Clarke (1987) for the stability and thickness of films, has not been developed.

As indicated in the introduction, the grain boundary structure is only considered from a geometrical point of view by determining misorientation axes/angle pairs. The results are interpreted in the framework of the coincidence site lattice model. Several different experimental approaches clearly show a relationship between grain boundary energy minima and the occurrence and frequency of CSL misorientations. For metals, ceramics and oxide superconductors, CSL misorientations are prominent (i) in textured materials (e.g. Randle and Ralph 1988; Zhu et al. 1991), (ii) in situations where grain boundaries intersecting a surface are free to rotate (Randle 1994) or rotating sphere experiments (e.g. Sutton and Balluffi 1987) (iii) for plate-like grains that are free to rotate (Zhu et al. 1994) or (iv) in bicrystal experiments with symmetrical tilt or twist boundaries (e.g. Sun an Balluffi 1982; Sutton and Balluffi 1987). Common to these experiments is that either the grains or grain boundaries are free to rotate, or special planes or directions have been preselected in the experiments. However, even under these idealised experimental conditions not all predicted CSL misorientations are observed and not all identified CSL misorientations necessarily have special properties due to the involvement of irrational or asymmetric grain boundary planes (e.g. Randle 1995). In dense, polycrystalline aggregates without preferred orientation, where grains are not free to rotate, even cubic materials like metals (Rabet et al. 1992) or MgO (Faul, unpublished data) do not show a preference for CSL misorientations.

Several studies point to the importance of grain boundary plane orientations and interplanar spacing in determining grain boundary properties. For example, Bouchet and Priester (1987) observed that at low impurity levels in polycrystalline nickel, segregations to grain boundaries are more dependent on the grain boundary plane orientation and planar atomic density than CSL orientations. Swiatnicki et al. (1995) found that in polycrystalline Al_2O_3 only a few misorientations corresponding to CSLs were present, but more frequently one of the grain surfaces at a two-grain boundary corresponded to a low index, dense crystallographic plane. Grain surfaces corresponding to low crystallographic index planes appear faceted when they are surrounded by melt; and similarly to our assumptions Swiatnicki et al. (1995) concluded that the growth of grains bordered by these planes is independent of the orientation relationships of neighbouring grains. These studies indicate that grain misorientations together with grain boundary plane orientations should be evaluated for a more complete assessment of grain boundary energies, but also that grain boundaries might have to be approached by considering the actual bond structure at the interface.

In conclusion, in polycrystalline olivine without preferred orientation the vast majority of grain boundaries are general grain boundaries with misorientations $>10°$. In partially molten aggregates where both wetted and melt-free grain boundaries occur, neighbouring grains with misorientation angles around 60° have a high probability of being melt-free, whereas wetted grain boundaries are equally probable between grains of all misorientations. Differences between the distributions and non-randomness of the distribution of melt-free grain boundaries indicate that the relative orientation of neighbouring grains is a factor relevant for the determination of the grain boundary structure and energy. The presumably small differences in grain boundary energy for different misorientations are not enough to lead to a preferred development of only a few special misorientations during grain growth, at least not for the starting material used here and in the absence of deformation. These results further support the notion that wetted grain boundaries are part of a stable, minimum energy texture and are therefore expected to be present in partially molten regions of the upper mantle.

Acknowledgements We thank David Vowles and Frank Brink for assistance with the electron microscopy as well as Bill Hibberson with the piston cylinder experiments. Martyn Drury suggested to examine CSL misorientations for the hcp structure of oxygen and provided a preprint of their manuscript. We thank David Mainprice and an anonymous reviewer for their thoughtful reviews; David Mainprice also calculated the texture index for our samples. Discussions with Martin Cmiral also helped to improve the manuscript.

References

Babcock SE, Vargas JL (1995) The nature of grain boundaries in the high–T_c superconductors. Ann Rev Mater Sci 25:193–222

Beere W (1975) A unifying theory of the stability of penetrating liquid phases and sintering pores. Acta Metall 23:131–138

Bollmann W (1982) Crystal lattices, interfaces, matrices. Published by the author, ETH Zürich

Bouchet D, Priester L (1987) Grain boundary plane and intergranular segregation in nickel-sulphur system. Scr Metall 21:475–478

Cheeney RF (1983) Statistical methods in geology. George Allen and Unwin, London

Clarke DR (1987) On the equilibrium thickness of intergranular glass phases in ceramic materials. J Am Ceram Soc 70:15–22

Cmíral M, Fitz Gerald JD, Faul UH, Green DH (1998) A close look at dihedral angles and melt geometry in olivine-basalt aggregates: a TEM study. Contrib Mineral Petrol 130:336–345

Cooper RF, Kohlstedt DL (1982) Interfacial energies in the olivine-basalt system. Adv Earth Planet Sci 12:217–229

Drury MR, Fitz Gerald JD (1996) Grain boundary melt films in an experimentally deformed olivine-orthopyroxene rock: implications for melt distribution in upper mantle rocks. Geophys Res Let 23:701–704

Farver JR, Yund RA, Rubie DC (1994) Magnesium grain boundary diffusion in forsterite aggregates at 1000°–1300°C and 0.1 to 10 GPa. J Geophys Res 99:19809–19819

Faul UH (1997) Permeability of partially molten upper mantle rocks from experiments and percolation theory. J Geophys Res 102: 10299–10311

Faul UH, Toomey DR, Waff HS (1994) Intergranular basaltic melt is distributed in thin, elongated inclusions. Geophys Res Lett 21:29–32

Fliervoet TF, Drury MR, Chopra PN (1998) Crystallographic preferred orientations and misorientations in olivine rocks deformed by diffusion or dislocation creep. In press Tectonophysics

Grimmer H (1979) The distribution of disorientation angles if all relative orientations of neighbouring grains are equally probable. Scr Metall 13:161–164

Grimmer H (1980) A unique description of the relative orientation of neighbouring grains. Acta Crystallogr A36:382–389

Goldstein H (1980) Classical mechanics. Addison-Wesley, Reading, Mass.

Kim D-Y, Wiederhorn SM, Hockey BJ, Handwerker CA, Blendell JE (1994) Stability and surface energies of wetted grain boundaries in aluminium oxide. J Am Ceram Soc 77:444–453

Laporte D (1994) Wetting behaviour of partial melts during crustal anatexis: the distribution of hydrous silicic melts in polycrystalline aggregates of quartz. Contrib Mineral Petrol 116:486–499

Laval JY, Swiatnicki W (1994) Atomic structure of grain boundaries in $YBa_2Cu_3O_{7-x}$. Physica C 221:11–19

Mainprice D, Lloyd GE, Casey M (1993) Individual orientation measurements in quartz polycrystals: advantages and limitations for texture and petrophysical property determinations. J Struct Geol 15:1169–1187

Morawiec A (1995) Misorientation-angle distribution of randomly oriented symmetric objects. J Appl Crystallogr 28:289–293

Poirier J-P (1975) On the slip systems of olivine. J Geophys Res 80:4059–4061

Priester L (1989) Geometrical speciality and special properties of grain boundaries. Rev Phys Appl 24:419–438

Rabet L, Kestens L, Van Houtte P, Aernoudt E (1992) Anomalous grain growth during decarbonisation of non oriented steel sheet. Mater Sci Forum 94–96:611–618

Randle V (1992) Microtexture determination and its applications. Institute of Materials, London

Randle V (1993) The measurement of grain boundary geometry (Electron Microscopy in Materials Science Series). Institute of Physics Publishing, Bristol

Randle V (1994) Asymmetric tilt boundaries in polycrystalline nickel. Acta Crystallogr A50:588–595

Randle V (1995) An investigation of grain-boundary plane crystallography in polycrystalline nickel. J Mater Sci 30:3983–3988
Randle V, Ralph B (1988) Local texture changes associated with grain growth. Proc R Soc London A415:239–256
Ricoult DL, Kohlstedt DL (1983a) Low-angle grain boundaries in olivine. In: Yan MF, Heuer AH (eds) Character of grain boundaries (Advances in Ceramics vol. 6). American Ceramic Society, Columbus, pp 59–72
Ricoult DL, Kohlstedt DL (1983b) Structural width of low-angle grain boundaries in olivine Phys Chem Minerals 9:133–138
Roberts JJ, Tyburczy JA (1991) Frequency dependent electrical properties of polycrystalline olivine compacts. J Geophys Res 96:16205–16222
Shaw TM, Duncombe PR (1991) Forces between aluminium oxide grains in a silicate melt and their effect on grain boundary wetting. J Am Ceram Soc 74:2495–2505
Sun CP, Balluffi RW (1982) Secondary grain boundary dislocations in [001] twist boundaries in MgO. Philos Mag A 46:49–62
Sutton AP, Balluffi, RW (1987) On geometric criteria for low interfacial energy. Acta Metall 35:2177–2201
Swiatnicki W, Lartigue-Korinek S, Laval JY (1995) Grain boundary structure and intergranular segregation in Al_2O_3. Acta Metall Mater 43:795–805
Tan BH, Jackson I, Fitz Gerald JD (1997) Shear wave dispersion and attenuation in fine-grained synthetic olivine aggregates: preliminary results. Geophys Res Lett 24:1055–1058
Vaughan PJ, Kohlstedt DL, Waff HS (1982) Distribution of the glass phase in hot-pressed olivine-basalt aggregates: An electron microscopy study. Contrib Mineral Petrol 81:253–261
Zhu Y, Zhang H, Wang H, Suenaga M (1991) Grain boundary in textured $YBa_2Cu_3O_{7-x}$ superconductor. J Mater Res 6:2507–2518
Zhu Y, Suenaga M, Sabatini RL (1994) Misorientation angle distributions for large-angle grain boundaries in $Bi_2Sr_2CaCu_2O_8$ and $Bi_2Sr_2Ca_2Cu_3O_{10}$ composite tapes. Appl Phys Lett 65:1832–1834